



Article

Europium-Doped Sol-Gel SiO₂-Based Glasses: Effect of the Europium Source and Content, Magnesium Addition and Thermal Treatment on Their Photoluminescence Properties

Hussein Fneich ^{1,3}, Nathalie Gaumer ², Stéphane Chaussement ², Wilfried Blanc ³ 
and Ahmad Mehdi ^{1,*} 

¹ University of Montpellier, ICGM, CMOS, CNRS UMR 5253, 34095 Montpellier Cedex 5, France; hussein.fneich@etu.umontpellier.fr

² Université d'Angers, LPhiA, UPRES EA 4464, 49045 Angers Cedex 01, France; nathalie.gaumer@univ-angers.fr (N.G.); stephane.chaussement@univ-angers.fr (S.C.)

³ Université Côte d'Azur, InPhyNi, CNRS UMR 7010, Parc Valrose, 06108 Nice, France; wilfried.blanc@unice.fr

* Correspondence: ahmad.mehdi@umontpellier.fr; Tel.: +33-(0)4-6714-3832

Received: 14 June 2018; Accepted: 16 July 2018; Published: 19 July 2018



Abstract: Rare-earth doped silica-based glasses lead the optical materials due to their tailorable spectroscopic and optical properties. In this context, we took advantage of the sol-gel process to prepare various Eu-doped silica glasses to study their luminescent properties before and after annealing at 900 °C. The effect of magnesium on these properties was studied in comparison with Mg-free-glass. Using TEM, nitrogen sorption, XRD and FT-IR, we confirmed that the magnesium modifies the glass structure and the thermal treatment eliminates the aqueous environment, modifying the structure ordering. The emission spectra and the decay time curves show the advantages of the Mg addition and the annealing on the photoluminescent properties.

Keywords: luminescent materials; sol-gel; silica; europium; magnesium; photoluminescence

1. Introduction

Silicate glasses are commonly used as optical materials in a broad range of applications due to their ready availability, relatively simple fabrication and large panel of properties (transparency, chemical durability, etc.) [1]. Their luminescent properties are usually modulated by doping with rare-earth ions. Since their discovery in the last years of the 18th century, rare earth elements have displayed wide applications, especially in photoluminescence [2–5]. Their exceptional spectroscopic properties coming from their 4f intra-configurational electronic transitions lead to high quantum efficiencies and narrow emission bands [4].

The simplicity of the sol-gel route in glass fabrication, the low temperature processing conditions, the large number of possibilities in material design and the highly concentrated and homogenous doping levels, make it more applied than conventional melt processing [6–8]. Then, rare-earth ion-doped sol-gel silicate glasses are considered promising materials for photonics applications such as lasers, photonics or fiber optics [7,9–11]. For decades, Eu³⁺ doped and co-doped sol-gel silica glasses have attracted particular interest for their optical properties. In particular, this rare-earth ion exhibits an intense red luminescence of interest for phosphors [3]. This ion is also well known in structural probes used to analyze materials' matrix structures [12–15].

Indeed, the Eu³⁺ emission spectrum is composed of several multiplet transitions $^5D_0 \rightarrow ^7F_J = 0,1, \dots, 6$ [16]. The spin-forbidden transitions $^5D_0 \rightarrow ^7F_0$ and $^5D_0 \rightarrow ^7F_2$ are strongly influenced

by the electrostatic local field of the luminescent site. On the contrary, the ${}^5D_0 \rightarrow {}^7F_1$ transition is mainly magnetic dipolar and intensity-insensitive to the local field. For these reasons, the analysis of the ${}^5D_0 \rightarrow {}^7F_{0,1,2}$ band shapes can provide relevant information on the local structure around the rare-earth ion [17]. Luminescent properties of rare-earth ions depend on many factors such as rare-earth ion concentrations, impurities (hydroxyl, etc.), atomic arrangement, etc. To improve the luminescent properties of europium ions, several co-dopants have been investigated [18]. Co-doping with aluminum has been extensively studied [19,20]. In this article, we focus our attention on europium-doped sol-gel glasses co-doped with magnesium.

Magnesium oxide, MgO, is miscible in silicate glasses and considered as one of the most important silicate glass network modifiers in order to increase the mechanical strength and chemical stability of glass [21,22], although, once its quantity exceeds 20 mol%, it starts to act as network former or intermediate [22–24]. Furthermore, the incorporation of MgO makes the glass network tighter and the network dimensionality lower without phase segregation. It also decreases the glass transition temperature (T_g) and increases the glass crystallization temperature (T_c). These actions broaden the glass sintering temperature window ($T_c - T_g$), leading to the inhibition of glass crystallization and enabling the sintering of the glass without crystalline phase formation. These effects are due to the fact the newly formed Si–O–Mg bonds are weaker than Si–O–Si bonds [22,25–28].

To the best of our knowledge, only one article has dealt with the optical properties of Eu^{3+} -doped sol-gel silica glass co-doped with magnesium [29]. This study reported an increase of the luminescence intensity of Eu^{3+} when magnesium was added compared to Mg-free silica, but these conclusions are based on the study of nanoparticles where surface effects can impact the luminescent properties. Moreover, luminescence decay curves were not measured, nor OH content.

In this work, we studied the effect of Eu(III) ions and their concentrations on the photoluminescent properties of doped silicate glass, by using two different salts: europium (III) chloride hexahydrate ($\text{EuCl}_3 \cdot 6\text{H}_2\text{O}$) and the europium (III) nitrate hexahydrate ($\text{Eu}(\text{NO}_3)_3 \cdot 6\text{H}_2\text{O}$), with three different molar contents: 0.2, 0.5 and 1 mol%. In addition, magnesium nitrate hexahydrate ($\text{Mg}(\text{NO}_3)_2 \cdot 6\text{H}_2\text{O}$) with 10 mol% was introduced in the silica matrix and its effect on the photoluminescence properties was studied. Finally, the heat treatment effect on the photoluminescence properties of the materials was investigated by annealing all samples at 900 °C. The thermal treatment of the materials has some significant effects on the silica structure, such as promoting the SiO_2 condensation in the three-dimensional network which lead to more organized structure after decreasing of the silanol group concentration (Si–OH) [30–33].

2. Results and Discussion

2.1. Structural Analysis

2.1.1. Characterization of the Porosity

All the samples were characterized by TEM. The TEM images for all samples are similar to those reported in the Figure 1 related to the $\text{SiEu}_{\text{Cl}}^{0.2}$ sample before and after thermal treatment. Before heat treatment, the texture of the as-prepared SiO_2 sol-gel powder is heterogeneous in terms of porosity (Figure 1a). The materials obtained after the hydrolysis and poly-condensation of silicon alkoxides are defined as xerogels, where few nm nanoparticles of SiO_2 are coalesced into larger agglomerates. After annealing at 900 °C, the structure looks more homogeneous (Figure 1b). The powdered microporous xerogel is transformed into a semi-densified silica powder.

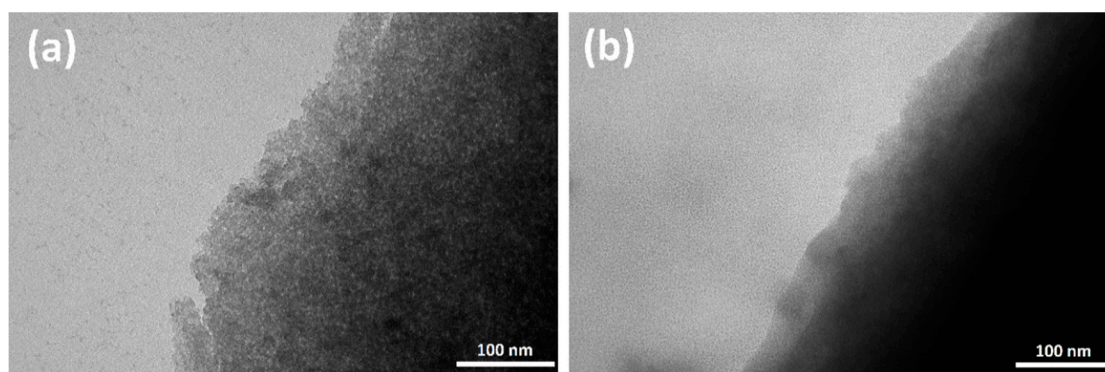


Figure 1. TEM images of $SiEu_{Cl}^{0.2}$ before (a) and after (b) thermal treatment at 900 °C.

To evaluate the change of the porosity, surface area and pore volume were measured by nitrogen sorption analysis (BET method). Results are reported in Table 1.

Table 1. BET surface area and pore volume for representative samples before and after annealing.

Sample	BET Surface Area m^2/g	Pore Volume cm^3/g
$SiEu_{Cl}^1$	334.0 ± 1.1	0.321
$SiEu_{Cl}^1 900$	212.9 ± 1.7	0.091
$SiEu_N^1$	306.9 ± 2.0	0.218
$SiEu_N^1 900$	142.8 ± 1.1	0.082
$SiMg_N^{10}Eu_N^1$	289.6 ± 2.3	0.519
$SiMg_N^{10}Eu_N^1 900$	52.4 ± 1.4	0.166

For all samples, heat treatment leads to a decrease of the BET surface area and the pore volume. While the BET surface areas are similar for all the as-prepared sol-gel glasses, the heat treatment is much more efficient to reduce the BET surface area when the sample contains magnesium. Indeed, in case of Mg-free silica, the surface area reduced after annealing by 36.2% and 53.4% for $SiEu_{Cl}^1$ and $SiEu_N^1$, respectively. This reduction is 82% for $SiMg_N^{10}Eu_N^1$. The same trends are observed for all the europium concentrations.

The incorporation of magnesium into silica tends to modify the structure of the glassy network. Less SiO_4 tetrahedra are connected, decreasing the viscosity of the glass [34]. This may explain the lower BET surface area observed for Mg-doped samples [35].

Regarding the pore volume, the addition of magnesium increases the pore volume. It is about two times higher compared to Mg-free glass. But, it reduces highly with the heat treatment for all samples. This reduction is 72%, 63% and 68% for $SiEu_{Cl}^1$, $SiEu_N^1$ and $SiMg_N^{10}Eu_N^1$ respectively, it proves the samples densification by heat treatment.

2.1.2. X-Ray Diffraction

To study the structural evolution as a function of the temperature, the samples were characterized by X-Ray Diffraction (XRD). XRD patterns of six samples are presented in the Figure 2. For all samples, the patterns contain the same features: (i) a broad band at $2\theta \approx 22^\circ$ and (ii) peaks at $\sim 44^\circ$. The broad band at $2\theta \approx 22^\circ$ is the fingerprint of the amorphous structure of the network [32,36]. After heat treatment, the position of this peak shifts to lower angle, from 23° to 21.5° . Such shift is usually attributed to a change of the silica network, making evidences of an amorphous structure ordering [32]. The peaks at $2\theta \approx 44^\circ$ correspond to an artifact, due to the sample holder. We do not observe the presence of α -quartz crystalline phase as reported by Bansal et al., nor $Mg(NO_3)_2 \cdot 6H_2O$, which was expected to be present only for nominal concentration higher than 15 mol% [37].

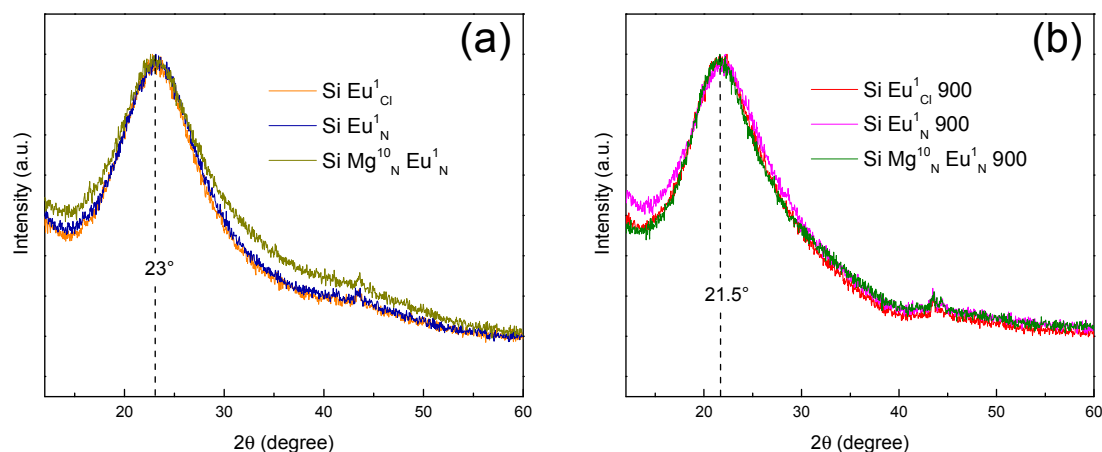


Figure 2. XRD patterns of (a) $SiMg_N^x Eu_z^1$ (b) $SiMg_N^x Eu_z^1 900$.

Otherwise, there is no presence of MgO corresponding peaks. Normally, MgO crystal shows three weak diffraction peaks around $2\theta = 36.9, 74.6,$ and 78.6° and two others around $2\theta = 42.8$ and 62.2° stronger than amorphous silica broad fuzzy diffraction lines [38–40].

2.1.3. FT-IR Analyses

As fast and non-destructive analysis technique, FTIR spectroscopy is known to detect the local changes and give information about the functional groups of the glass structure. Therefore, we have recorded the FTIR spectra for the studied samples (Figure 3). All these bands can be associated to the SiO_2 network and the presence of OH groups.

First of all, it is worth presenting some specific bands of IR spectra of the SiO_2 based compounds and the information they gave. Three vibrational modes of the Si–O–Si group are mainly present in the region between 400 and 1300 cm^{-1} . A strong peak near 450 cm^{-1} (labeled “1” in the Figure 3) is assigned to a mode called rocking mode or rocking motion that proves the silicate’s three-dimensional network presence in the glass. The oxygen atom, bridging two adjacent silicon atoms forming siloxanes bonds (Si–O–Si), vibrates perpendicularly to the Si–O–Si plane [41–46]. The next one, a weaker band around 800 cm^{-1} (labeled “2”) is associated to a symmetric stretching mode, a vertical motion of the oxygen atoms in the Si–O–Si plane [41–45]. Finally, a strong band around 1100 cm^{-1} (labeled “4”) is assigned to the Si–O–Si asymmetric stretching mode where the bridging oxygen atoms move horizontally in to the Si–O–Si plane [41–45]. In addition, the shoulder at about 1200 cm^{-1} is generally interpreted as a sign of the amorphous network of SiO_2 [30].

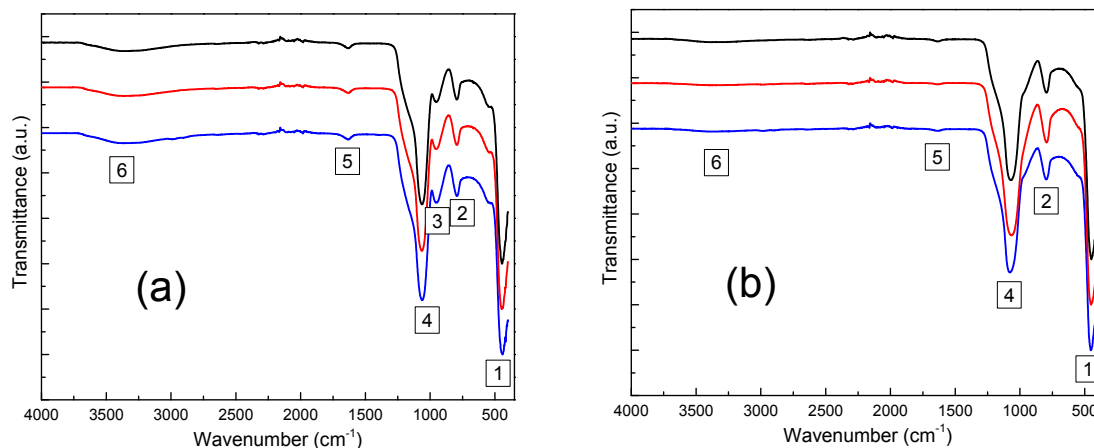


Figure 3. Cont.

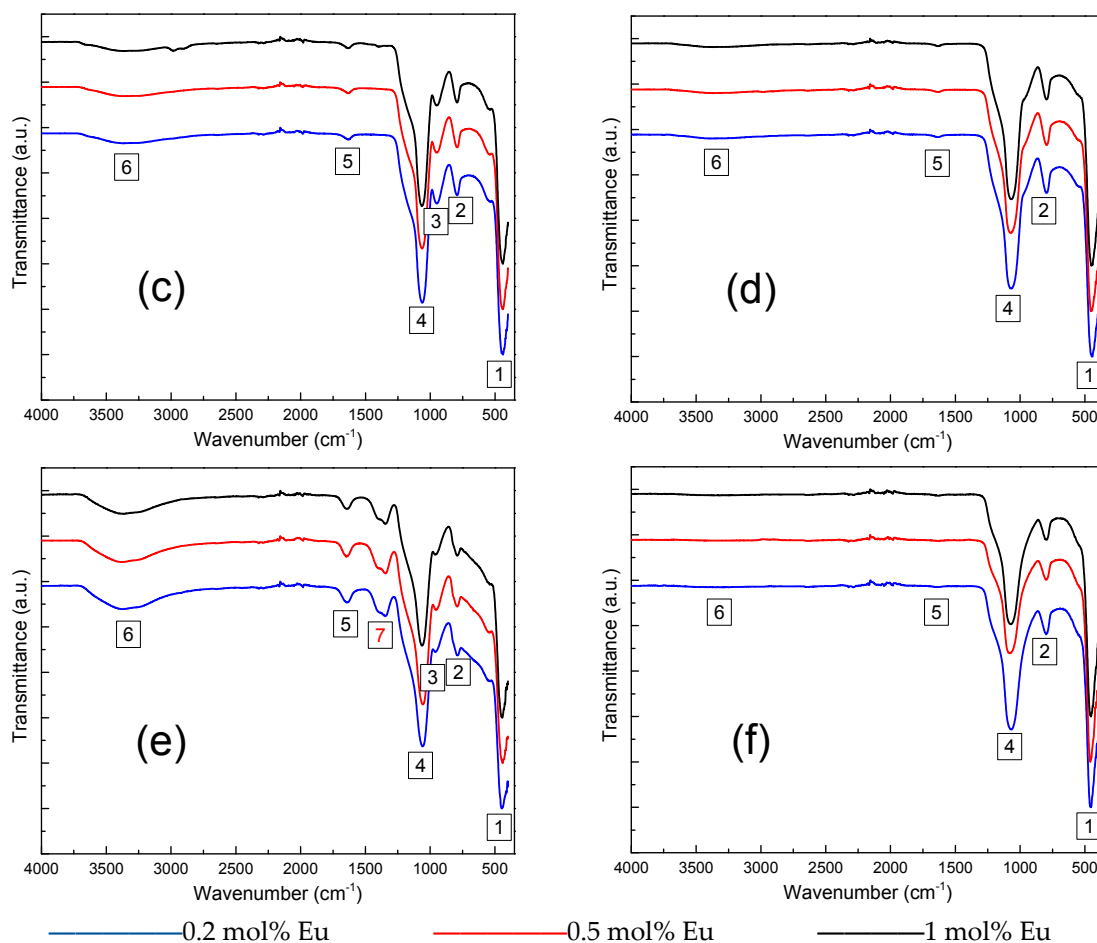


Figure 3. Room temperature FT-IR spectra of (a) $SiEu_{Cl}^y$ (b) $SiEu_{Cl}^y$ 900 (c) $SiEu_N^y$ (d) $SiEu_N^y$ 900 (e) $SiMg_N^{10}Eu_N^y$ (f) $SiMg_N^{10}Eu_N^y$ 900.

The IR bands associated to the presence of OH group are labeled 3, 5 and 6 in Figure 3. In the spectra of non-annealed materials, the low frequency band around 950 cm^{-1} (“3”) is assigned to the Si–OH symmetric stretching vibrations [43,44,47]. The other low frequency band around 1650 cm^{-1} (“5”) is attributed to the bending vibration of adsorbed molecules of water H_2O [43,44] which confirm that the broad band between $3000\text{--}3650\text{ cm}^{-1}$ (“6”) owes to an overlap of the O–H stretching vibrations in H-bonded molecular water adsorbed by the samples ($3300\text{--}3500\text{ cm}^{-1}$) and the H stretching of Si–OH groups inside of the glass (around 3650 cm^{-1}) [43,44,48].

Before thermal treatment, all the samples exhibit IR bands associated to the presence of OH groups (bands 3, 5 and 6). Comparing the spectra in Figure 3a–d, there are no differences in the positions and shapes of the peaks for the samples with different europium complexes and quantities, both before and after annealing at $900\text{ }^\circ\text{C}$. The samples containing magnesium exhibit higher content of OH groups (Figure 3e). This could be due to the presence of magnesium nitrate which is hexahydrated. After annealing at $900\text{ }^\circ\text{C}$, the OH-related bands decrease strongly and almost disappear.

These results are confirmed by the elementary analysis with 1.76 wt.%, 1.82 wt.% and 2.96 wt.% of hydrogen in $SiEu_{Cl}^x$, $SiEu_N^x$ and $SiMg_N^{10}Eu_N^x$ respectively and 1.22 wt.%, 1.19 wt.% and 0.4 wt.% after thermal treatment of the respective materials. Therefore, we noticed a decreasing by 31 wt.%, 34 wt.% and 86 wt.% of hydrogen quantities after annealing of $SiEu_{Cl}^x$, $SiEu_N^x$ and $SiMg_N^{10}Eu_N^x$ respectively. We can observe that the liberation of the OH groups easier after the Mg addition that led to a more open structure seen by the higher pore volume compared to Mg-free-glass. The origin of the residual

traces of water in the annealed samples is not clear and could be due to adsorbed water from the ambient atmosphere during the preparation for the different analyses [37].

Finally, a peak between 1350–1400 cm^{-1} (labeled “7”) is present only for the silica containing magnesium before annealing (Figure 3f). It is assigned to the presence of NO_3^- ions in the glassy network [37,49]. This IR peak disappears after annealing at 900 °C, which indicates the decomposition of these ions at high temperature.

2.2. Photoluminescence Study

2.2.1. Emission Spectra

The Eu^{3+} emission spectrum is composed of several multiplet transitions $^5\text{D}_0 \rightarrow ^7\text{F}_{J=0,1,\dots,6}$ [16]. The highest energy one, $^5\text{D}_0 \rightarrow ^7\text{F}_0$, is spin-forbidden and only allowed by J -mixing effects [16,50]. The shape and the position of the associated spectral band are strongly influenced by the electrostatic local field of the luminescent site. The second transition, $^5\text{D}_0 \rightarrow ^7\text{F}_1$, is mainly magnetic dipolar and intensity-insensitive to the local field, but its splitting feature directly depends on the crystal field experienced by the luminescent site [16,51]. For this reason, the analysis of the $^5\text{D}_0 \rightarrow ^7\text{F}_1$ band shape can provide relevant information on the local structure around the rare-earth ion [17]. The intensity of this band is also used as a reference to normalize and compare different emission spectra. The intensity and the 5-fold splitting of the $^5\text{D}_0 \rightarrow ^7\text{F}_2$ transition both depend drastically on the crystal field strength [16,52]. Its band shape is therefore trickier to analyze and to link with the structure of the luminescent site. Figure 4 displays the emission spectra of the different samples and allows observing the effects of the thermal treatment, of the Eu^{3+} doping concentration, of the Mg co-doping and of the Eu^{3+} -salt used in the sol-gel process. All spectra were recorded at room temperature and the intensities were normalized to the $^5\text{D}_0 \rightarrow ^7\text{F}_1$ emission.

Considering samples before the thermal treatment (Figure 4a), the most drastic effect is due to the Mg co-doping. Independently of the Eu^{3+} concentration and for both Eu^{3+} salts, the emission spectra of the Mg-free samples are very similar: the inhomogeneous line broadening is weak for the $^5\text{D}_0 \rightarrow ^7\text{F}_0$ and $^5\text{D}_0 \rightarrow ^7\text{F}_1$ emission bands, which is typical of the luminescent ion in an aqueous environment where the sites are similar and composed of OH groups [53]. On the contrary, one can observe from the emission spectrum of the co-doped sample that Mg allows an inhomogeneous line broadening, even for the lowest Eu^{3+} doping concentration. This result is surprising because it was measured by elementary analysis a hydrogen content before thermal treatment higher in the Mg co-doped sample (2.96 wt.%) than in the Mg-free samples (1.76 wt.% and 1.82 wt.%). It means that a specific structural organization in the Mg co-doped sample prevents OH groups from affecting the Eu^{3+} emission properties. Furthermore, one can compare the symmetry of the luminescent sites in comparing the intensities of the dipolar electric transition $^5\text{D}_0 \rightarrow ^7\text{F}_2$ and of the dipolar magnetic transition $^5\text{D}_0 \rightarrow ^7\text{F}_1$. Indeed, lowering of inversion symmetry leads to a mixing of different parity states, thus allowing electric dipolar transitions. Consequently, low value of the peak intensity ratio $R = I(^5\text{D}_0 \rightarrow ^7\text{F}_2) / I(^5\text{D}_0 \rightarrow ^7\text{F}_1)$ is indicative of high symmetry sites, whereas high value of R is indicative of a distribution of different distorted sites [53]. The maximum intensity is considered as of the highest point of each peak. From spectra of Figure 4a, before thermal treatment, it was calculated R values ranging from 2.2 to 3.6 for the Mg-free samples, whereas R varies from 5.0 to 6.9 in the Mg co-doped samples. Because an aqueous environment allows high symmetry sites for the luminescent ions [54], these results are indicative of the presence of OH groups around Eu^{3+} in the Mg-free samples. On the contrary, a large diversity of low-symmetry sites in the Mg co-doped samples can be corroborated by large R values and the inhomogeneous line broadening observed from the emission spectra.

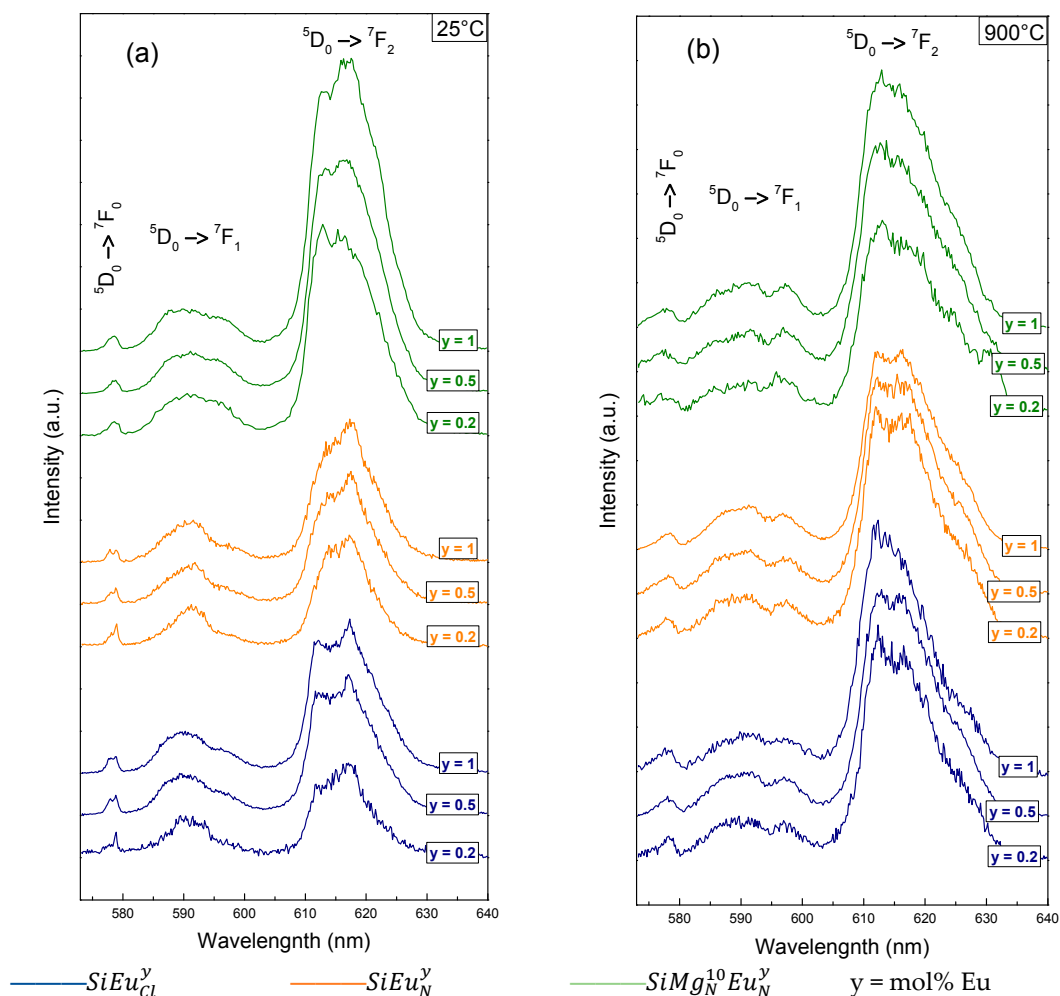


Figure 4. Room temperature emission spectra of the different samples (a) before and (b) after the thermal treatment at 900 °C (Intensities are normalized to the maximum of the ${}^5D_0 \rightarrow {}^7F_1$ emission band).

Whether for thermally treated samples or for untreated ones (Figure 4a,b), no clear trend can be observed on the emission spectra by varying the Eu^{3+} doping concentration from 0.2 to 1 mol%. Only a slight increase of the inhomogeneous line broadening, together with a weak increase of the R ratio, can be observed for the higher Eu^{3+} concentration. It means that there are no drastic structural modifications and that an increase of the doping level does not lead to a rare-earth clustering trend (at least up to the highest concentration used in this study) but only to an enhancement of the structural diversity of the luminescent sites.

The use of a nitrate or a chloride europium salt also weakly impacts the emission spectra: all Mg-free samples globally display similar spectra, whether for thermally treated samples or for untreated ones. Only small differences can be observed between spectra of Mg-free samples before the thermal treatment. Nitrate ion is known to easily form europium complexes and it can affect the close environment of the europium ions, especially in making more difficult the solvent removal during the drying stage of the sol-gel process. This can therefore explain the fact that the SiEu_N^y samples at 25 °C give emission spectra more like those obtained from Eu^{3+} in an aqueous environment. Anyway, the thermal treatment at 900 °C clearly cancels any effect of the europium salt on the emission spectra and therefore on the local environment of the rare-earth ions (SiEu_N^y and SiEu_{Cl}^y samples in Figure 4b).

The effect of the thermal treatment is drastic on the emission spectra for all samples. Normally, the presence of OH groups creates fluorescence quenching due to the non-radiative de-excitation of

Eu^{3+} ions caused by the energy transfer to OH vibration, while the heat treatment dehydrate and condensate the glass and lead to better integration of Eu^{3+} ions in the glassy structure and better fluorescence [55]. Especially in Mg-free samples, one can observe an inhomogeneous line broadening together with an increase of the R ratio. This behavior is typical of the removal of the solvents and is commonly interpreted as a change from an aqueous environment to a cationic dominated one around the rare-earth ion: luminescent sites become more various and distorted with low symmetry [20]. For the Mg co-doped samples, the thermal treatment enhances the inhomogeneous line broadening that is already observed from the untreated samples. One can therefore suppose that the thermal treatment fully acts on the structure and/or on the structural diversity of the luminescent sites which are already free of solvent. Since at the same time the hydrogen content measured by elementary analysis is highly decreased by the thermal treatment (from 2.96 wt.% to 0.4 wt.%), one can assume that OH groups are not initially located within the close environment of the rare-earth ions in the Mg co-doped samples.

2.2.2. Decay Curves and Lifetimes

The luminescence decay curves of the $^5\text{D}_0$ level were recorded for all samples at the wavelength corresponding to the maximum intensity of the $^5\text{D}_0 \rightarrow ^7\text{F}_2$ emission band. Figure 5 displays the decay curves before and after the thermal treatment at 900 °C.

An important effect of an aqueous environment is the quenching of luminescence of Eu^{3+} ions [20]. In general, the organic residuals have high vibration frequencies and can efficiently quench luminescence of optically active ions. It is reported that the OH vibration frequency can be as high as 3340 cm^{-1} [56] so that only five phonons are needed to bridge the excited state $^5\text{D}_0$ and the ground state $^7\text{F}_j$ levels of Eu^{3+} . As a result, the presence of OH group near Eu^{3+} ions provide a nonradiative relaxation pathway and causes fluorescence quenching. On the other hand, thermal treatment can reduce or eliminate residual hydroxyl and other organic groups in the samples, reducing OH vibration quenching, and consequently increase the decay time. So, the lifetime increases with the thermal treatment at 900 °C for all samples is due to the reduction of the quenching centers.

Except for the $\text{SiMg}_{10}\text{Eu}_N^y$ samples treated at 900 °C, all samples show decay curves that are not single-exponential. These decay curves could be fitted with a 2-exponential curve but the origin of the two lifetime constants is not clear. For this study, we focus our attention on the comparison between all samples. Then, lifetimes were estimated in calculating an average value as:

$$\tau = \int I(t)tdt / \int I(t)dt \quad (1)$$

where $I(t)$ is the intensity decay profile. Obtained values are reported in Table 2.

Comparing the decay curve profiles (Figure 5) and the average lifetimes (Table 2) for all samples, one can observe that the Eu^{3+} dopant concentration has no significant effect. This is in agreement with the observations made from the emission spectra and it confirms that, up to 1 mol%, there is no concentration quenching of the luminescence which is generally attributed to the conjunction of rare-earth clustering with energy transfers between clustered ions by a cross-relaxation mechanism or phonon-assisted energy transfer [19].

The effect of the europium salt is also weak whether for thermally treated Mg-free samples or for untreated ones. The mean difference between SiEu_N^y and $\text{SiEu}_{\text{Cl}}^y$ samples is that the thermal treatment is slightly more effective on the lifetime lengthening by using a europium chloride salt: in average, the lifetime is multiplied by about 10 and 6 for $\text{SiEu}_{\text{Cl}}^y$ and SiEu_N^y samples, respectively. It confirms accordingly that the solvent removal around the rare-earth ions is more difficult by using a nitrate salt.

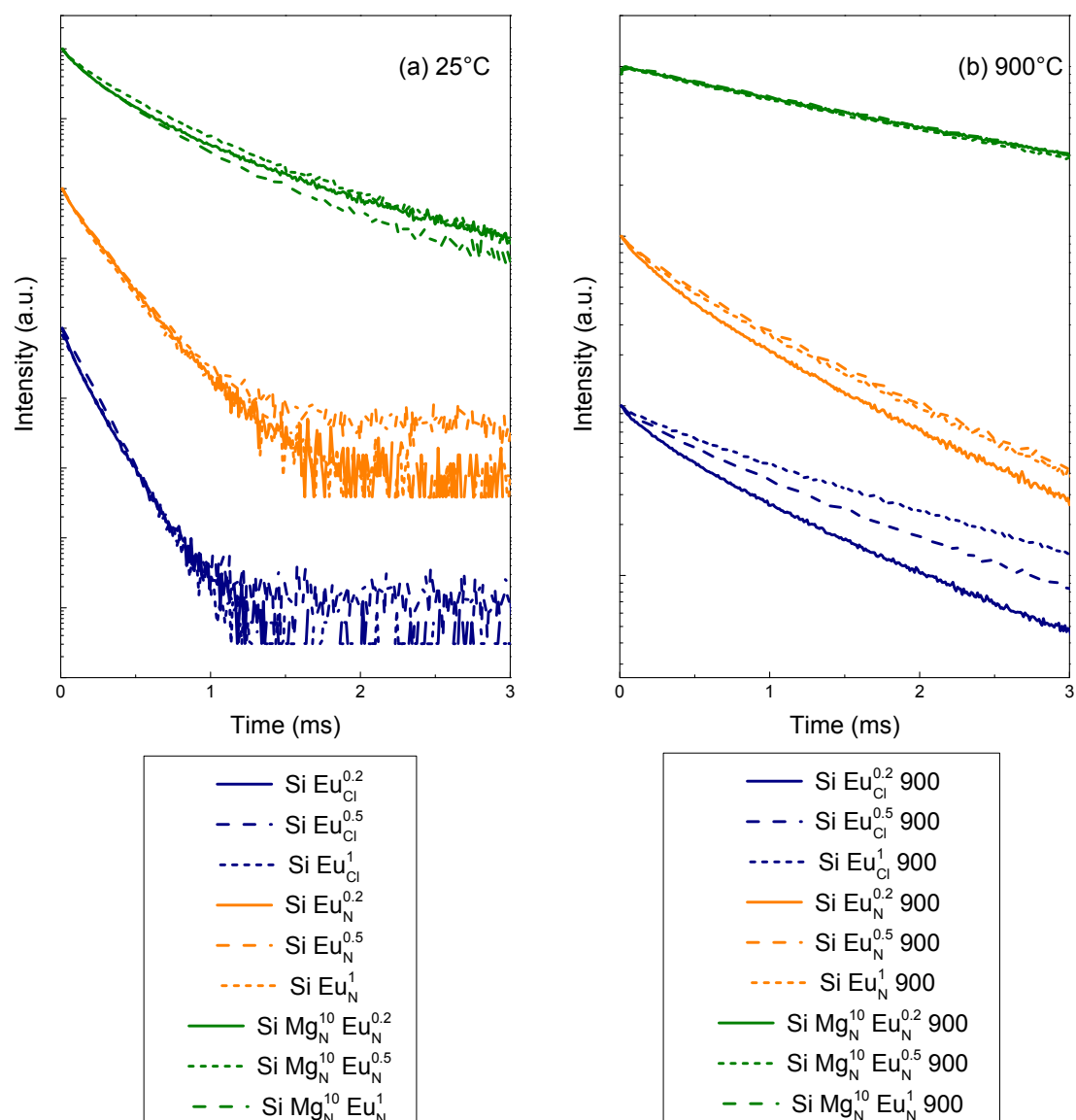


Figure 5. Luminescence decay curves of the 5D_0 level of Eu^{3+} measured at the maximum intensity of the $^5D_0 \rightarrow ^7F_2$ emission band (615 nm) for the different samples (a) before and (b) after the thermal treatment at 900 °C.

Table 2. Average lifetime τ of the 5D_0 level for the different samples before and after thermal treatment at 900 °C.

Samples		τ (ms)	
		25° C	900 °C
$\text{SiEu}_{\text{Cl}}^y$	$y = 0.2$ mol%	0.11	1.03
	$y = 0.5$ mol%	0.12	1.42
	$y = 1.0$ mol%	0.13	1.22
SiEu_{N}^y	$y = 0.2$ mol%	0.16	0.87
	$y = 0.5$ mol%	0.16	0.98
	$y = 1.0$ mol%	0.15	0.96
$\text{SiMg}_{\text{N}}^{10}\text{Eu}_{\text{N}}^y$	$y = 0.2$ mol%	0.40	1.80
	$y = 0.5$ mol%	0.42	1.80
	$y = 1.0$ mol%	0.34	1.78

As observed from the emission spectra, the effect of Mg on the decay curves and lifetimes is striking. Before the thermal treatment, the $SiMg_N^{10}Eu_N^y$ samples provide decay curves which are strongly non-exponential, with corresponding lifetimes three times longer than those obtained from Mg-free samples. In a previous study [20], it has been shown that a progressive increase of the thermal treatment temperature leads to a progressive evolution from a fast almost exponential decay (0.15 ms) to a slower almost exponential decay (1.5 ms) in a Eu^{3+} -doped silica gel. In the same study [20], an Al codoping together with a progressive thermal treatment allowed to reach longer lifetimes (up to 2.2 ms at 800 °C) associated with non-exponential decay curves. In the present study, without any thermal treatment, the Mg co-doping allows also a lengthening of the lifetime (from 0.15 ms to 0.42 ms) and leads also to non-exponential decay curves. This can be considered as an additional evidence of OH groups that are initially rarely located within the close environment of the rare-earth ions in the Mg co-doped samples. The thermal treatment at 900 °C of the Mg co-doped samples completes the solvent removal and provides luminescent sites with reduced nonradiative relaxation pathway since the lifetimes are about 80% longer than in the Mg-free samples.

3. Materials and Methods

3.1. Samples Preparation

Europium and magnesium doped silica bulks were synthesized by sol-gel process (inorganic polymerization). A summary of the preparation method with the final materials names are presented in Figure 6.

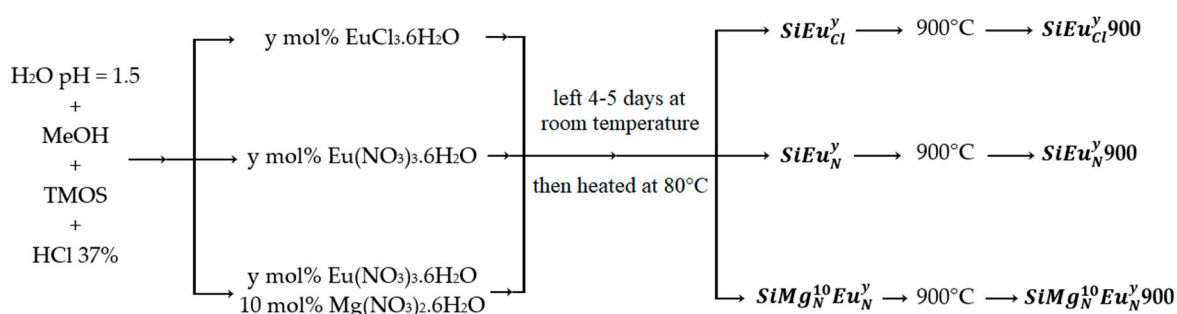


Figure 6. The main preparation route of the different glasses. The bolded names correspond to the nomenclature of the samples.

First, appropriate amounts of $EuCl_3 \cdot 6H_2O$, $Eu(NO_3)_3 \cdot 6H_2O$ and $Mg(NO_3)_2 \cdot 6H_2O$, purchased from Sigma-Aldrich (Saint-Quentin-Fallavier, France), were dissolved in 5 mL of acidic water with $pH = 1.5$. It worth noting that the acidic water ($pH = 1.5$) was prepared by placing 2.4 mL of HCl (37%, density 1.3 g/mL) in a 1 L Erlenmeyer flask which had been filled with ultra-pure water in order to obtain an acidic solution with $[H^+] = 0.0315$ mol/L, where the $pH = -\log(0.0315) = 1.5$. After their total dissolution, 5 mL of methanol (CH_3OH) were added, followed by 3.64 g (0.024 mol) of tetramethylorthosilicate (TMOS). The obtained mixture was stirred for 10–15 min at room temperature to hydrolyze the SiOMe into SiOH groups. Then, 4–5 drops of 37% hydrochloric acid (HCl) were added in order to decrease the pH permitting the polymerization take place. After stirring for 6 h, the mixture was left for several days under air at room temperature until obtaining dry pieces of glasses, which were grinded in a fine white powder and heated to 80 °C under air for 18 h to make sure of the total evaporation of all solvents. In order to study the effect of the thermal treatment, the half of the obtained powder of each sample was heated to 900 °C for 5 h using a heating rate of 10 °C/min. The different starting compositions of the studied materials are given in Table 3.

Table 3. Starting composition and nomenclature of mixed oxide.

Sample	EuCl ₃ ·6H ₂ O mol%	Eu(NO ₃) ₃ ·6H ₂ O mol%	Mg(NO ₃) ₂ ·6H ₂ O mol%	TMOS mol%
SiEu _{Cl} ^{0.2}	0.2	-	-	99.8
SiEu _{Cl} ^{0.5}	0.5	-	-	99.5
SiEu _{Cl} ¹	1	-	-	99
SiEu _N ^{0.2}	-	0.2	-	99.8
SiEu _N ^{0.5}	-	0.5	-	99.5
SiEu _N ¹	-	1	-	99
SiMg _N ¹⁰ Eu _N ^{0.2}	-	0.2	10	89.8
SiMg _N ¹⁰ Eu _N ^{0.5}	-	0.5	10	89.5
SiMg _N ¹⁰ Eu _N ¹	-	1	10	89

The main nomenclature is $SiMg_z^x Eu_z^y$ where “x” and “y” are the molar percentages of the magnesium and europium, respectively, and “z” is the salt source (“N” for nitrate and “Cl” for chloride). As an example, the $SiMg_N^{10} Eu_N^{0.2}$ contains 89.8 mol% SiO₂, 10 mol% MgO (from Mg(NO₃)₂·6H₂O) and 0.2 mol% Eu₂O₃ (from Eu(NO₃)₃·6H₂O).

3.2. Characterization Techniques

Transmission electron microscopy (TEM) images were taken using a 1200EX2 electron microscope operating (JEOL, Tokyo, Japan) at an acceleration tension of 100 kV equipped with an EMSIS camera mounted with an 11-megapixel CCD sensor (EMSIS GmbH, Muenster, Germany).

N₂ Physisorption experiments were carried out at −196 °C on a TriStar 3000 instrument (Micromeritics, Norcross, GA, USA). Samples were outgassed under vacuum at 150 °C over-night. Equivalent BET specific surface areas were determined in the relative pressure range P/P_0 from 0.01 to 0.3 using 74 points. The total pore volume was measured at $P/P_0 > 0.985$.

X-Ray Diffraction (XRD) experiments were performed using an X’Pert MPD θ - θ diffractometer (Philips, Amsterdam, Netherlands) with Cu K α radiation ($\lambda = 1.5418 \text{ \AA}$). It is equipped with the X’Celerator detector and nickel filter. Analyses were carried out between 12°–60° as interval with a step size of 0.033.

Fourier-Transform Infra-Red (FTIR) analysis was carried out in the range 400–4000 cm^{−1} using a Spectrum Two™ spectrometer (Perkin Elmer, Waltham, MA, USA) in Attenuated Total Reflectance (ATR) mode. The spectra were obtained from the accumulation of 10 scans with a used resolution of 2 cm^{−1}.

Elementary analysis was carried out with a Vario Micro Cube (Elementar, Munich, Germany) equipped with a UMX5 Comparator (Mettler Toledo, Zurich, Switzerland) balance with a 0.1 μg precision. The samples were combusted at 1150 °C to form an H₂O gas. The mass percentages measurement of hydrogen is detected by a thermal conductivity detector (TCD) katharometer (Elementar Americas Inc., Ronkonkoma, NY 11779, USA).

A pulsed doubled Nd:YAG laser (Spectra-Physics, Santa Clara, CA, USA) emitting at 532 nm with 10 Hz frequency was used as excitation source for the photoluminescence and lifetime measurements of europium. All measurements were performed with a photon counting device (Stanford Research Systems, Sunnyvale, CA, USA) at room temperature. The decay curves were carried out around the maximum of the emission line of europium with temporal window width of 10.24 μs .

4. Conclusions

In this article, the influence of Eu content and precursor, and the thermal treatment on the photoluminescent properties of Eu³⁺ were studied. Aluminum was used in many works to improve the luminescent properties of rare-earth ions in silica-based materials, but we focus our attention on an alternative element, magnesium. Mg-free samples have similar luminescent properties for all the europium concentrations. The annealing at 900 °C of europium-doped silica glass increases fluorescence lifetimes by removing aqueous sites and modifying the crystal field. Generally, the addition of magnesium is beneficial for luminescent properties. Both in the xerogel and in the

calcined material, lifetime is improved by adding magnesium, despite a higher content of OH groups. Calcination of Mg-glass leads to a highly radiative material with a longer lifetime.

Author Contributions: Conceptualization, A.M. and W.B.; Data curation, H.F., N.G. and S.C.; Formal analysis, H.F. and S.C.; Funding acquisition, W.B.; Investigation, H.F., S.C., W.B. and A.M.; Methodology, H.F., W.B. and A.M.; Software, H.F., N.G. and S.C.; Supervision, W.B. and A.M.; Validation, W.B. and A.M.; Visualization, W.B. and A.M.; Writing—original draft, H.F.; Writing—review & editing, S.C., W.B. and A.M.

Funding: This research was funded by Agence Nationale de la Recherche (ANR) grant number ANR-14-CE07-0016-01 (project Nice-DREAM).

Acknowledgments: The authors acknowledge the CNRS and the National Agency for Research (ANR) for their financial support to the project Nice-DREAM (ANR-14-CE07-0016-03).

Conflicts of Interest: The authors declare no conflict of interest.

References

1. Zarzycki, J. *Glasses and Amorphous Materials*; Wiley-VCH: Weinheim, New York, NY, USA, 1991; Volume 9, p. 798.
2. Henderson, B.; Imbush, G.F. *Optical Spectroscopy of Inorganic Solids*; Oxford University Press: Oxford, UK, 1989; p. 658.
3. Blasse, G.; Grabmaier, B.C. *Luminescent Materials*; Springer-Verlag: Berlin, Germany, 1994; p. 242.
4. Binnemans, K. Lanthanide-based luminescent hybrid materials. *Chem. Rev.* **2009**, *109*, 4283–4374. [[CrossRef](#)] [[PubMed](#)]
5. Dwivedi, Y.; Zilio, S.C. Advances in rare earth spectroscopy and applications. *J. Nanosci. Nanotechnol.* **2014**, *14*, 1578–1596. [[CrossRef](#)] [[PubMed](#)]
6. Brinker, C.J.; Scherer, G.W. *Sol-Gel Science: The Physics and Chemistry of Sol-Gel Processing*; Academic Press: San Diego, CA, USA, 1990; p. 912.
7. Klein, L.C. *Sol-gel optics: Processing and Applications*; Kluwer Academic: Boston, MA, USA, 1994; p. 598.
8. Yamane, M.; Asahara, Y. *Glasses for Photonics*; Cambridge University Press: Cambridge, UK, 2000; p. 283.
9. El-Hamzaoui, H.; Bigot, L.; Bouwmans, G.; Razdobreev, I.; Bouazaoui, M.; Capoen, B. From molecular precursors in solution to microstructured optical fiber: A sol-gel polymeric route. *Opt. Mater. Express* **2011**, *1*, 234–242. [[CrossRef](#)]
10. Vasconcelos, H.C.; Pinto, A.S. Fluorescence properties of rare-earth-doped sol-gel glasses. In *Recent Applications in Sol-Gel Synthesis*; Chandra, U., Ed.; InTech: Rijeka, Croatia, 2017; pp. 81–107.
11. Blanc, W. Luminescence properties of rare earth ions doped in insulating nanoparticles embedded in glassy hosts. In *From Glass to Crystal: Nucleation, Growth and Phase Separation: From Research to Applications*; Neuville, D.R., Cormier, L., Caurant, D., Montagne, L., Eds.; EDP Sciences: Les Ulis, France, 2017; pp. 433–449.
12. Ferrari, M.; Campostrini, R.; Carturan, G.; Montagna, M. Spectroscopy of trivalent europium in gel-derived silica glasses. *Philos. Mag. B* **1992**, *65*, 251–260. [[CrossRef](#)]
13. Elbanowski, M.; Makowska, B. The lanthanides as luminescent probes in investigations of biochemical systems. *J. Photochem. Photobiol. A* **1996**, *99*, 85–92. [[CrossRef](#)]
14. Streck, W.; Sokolnicki, J.; Legendziewicz, J.; Maruszewski, K.; Reifeld, R.; Pavich, T. Optical properties of Eu(III) chelates trapped in silica gel glasses. *Opt. Mater.* **1999**, *13*, 41–48. [[CrossRef](#)]
15. Alombert-Goget, G.; Gaumer, N.; Obriot, J.; Rammal, A.; Chausseant, S.; Monteil, A.; Portales, H.; Chiasera, A.; Ferrari, M. Aluminum effect on photoluminescence properties of sol-gel-derived Eu³⁺-activated silicate glasses. *J. Non-Cryst. Solids* **2005**, *351*, 1754–1758. [[CrossRef](#)]
16. Binnemans, K. Interpretation of Europium(III) spectra. *Coord. Chem. Rev.* **2015**, *295*, 1–45. [[CrossRef](#)]
17. Monteil, A.; El-Jouad, M.; Alombert-Goget, G.; Chausseant, S.; Gaumer, N.; Mahot, A.; Chiasera, A.; Jestin, Y.; Ferrari, M. Relationship between structure and optical properties in rare earth-doped hafnium and silicon oxides: Modeling and spectroscopic measurements. *J. Non-Cryst. Solids* **2008**, *354*, 4719–4722. [[CrossRef](#)]
18. Costa, V.C.; Lochhead, M.J.; Bray, K.L. Fluorescence line-narrowing study of Eu³⁺-doped sol-gel silica: Effect of modifying cations on the clustering of Eu³⁺. *Chem. Mater.* **1996**, *8*, 783–790. [[CrossRef](#)]
19. Lochhead, M.J.; Bray, K.L. Rare-earth clustering and aluminum codoping in sol-gel silica: Investigation using Europium(III) fluorescence spectroscopy. *Chem. Mater.* **1995**, *7*, 572–577. [[CrossRef](#)]

20. Monteil, A.; Chaussedent, S.; Alombert-Goget, G.; Gaumer, N.; Obriot, J.; Ribeiro, S.J.L.; Messaddeq, Y.; Chiasera, A.; Ferrari, M. Clustering of rare earth in glasses, aluminum effect: Experiments and modeling. *J. Non-Cryst. Solids* **2004**, *348*, 44–50. [[CrossRef](#)]
21. Pedone, A.; Malavasi, G.; Menziani, M.C.; Segre, U.; Cormack, A.N. Role of magnesium in soda-lime glasses: Insight into structural, transport, and mechanical properties through computer simulations. *J. Phys. Chem. C* **2008**, *112*, 11034–11041. [[CrossRef](#)]
22. Watts, S.J.; Hill, R.G.; O'Donnell, M.D.; Law, R.V. Influence of magnesia on the structure and properties of bioactive glasses. *J. Non-Cryst. Solids* **2010**, *356*, 517–524. [[CrossRef](#)]
23. Kuryaeva, R.G. The state of magnesium in silicate glasses and melts. *Glass Phys. Chem.* **2009**, *35*, 378–383. [[CrossRef](#)]
24. Kuryaeva, R.G. Compressibility of magnesium silicate glasses in comparison with those of aluminosilicate glasses. *Solid State Sci.* **2013**, *24*. [[CrossRef](#)]
25. Verné, E.; Bretcanu, O.; Balagna, C.; Bianchi, C.L.; Cannas, M.; Gatti, S.; Vitale-Brovarone, C. Early stage reactivity and in vitro behavior of silica-based bioactive glasses and glass-ceramics. *J. Mater. Sci. Mater. Med.* **2009**, *20*, 75–87. [[CrossRef](#)] [[PubMed](#)]
26. Ma, J.; Chen, C.Z.; Wang, D.G.; Jiao, Y.; Shi, J.Z. Effect of magnesia on the degradability and bioactivity of sol-gel derived SiO₂–CaO–MgO–P₂O₅ system glasses. *Colloids Surf. B Biointerf.* **2010**, *81*, 87–95. [[CrossRef](#)] [[PubMed](#)]
27. Diba, M.; Tapia, F.; Boccaccini, A.R.; Strobel, L.A. Magnesium-containing bioactive glasses for biomedical applications. *Int. J. Appl. Glass Sci.* **2012**, *3*, 221–253. [[CrossRef](#)]
28. Karpukhina, N.; Hill, R.G.; Law, R.V. Crystallisation in oxide glasses—A tutorial review. *Chem. Soc. Rev.* **2014**, *43*, 2174–2186. [[CrossRef](#)] [[PubMed](#)]
29. Onani, M.O.; Mushonga, P.; Koa, L.F.; Dejene, F.B. Luminescence properties of Eu- and Mg-codoped sol-gel SiO₂ glasses. *ISRN Nanotechnol.* **2012**, *2012*, 1–5. [[CrossRef](#)]
30. Lifshits, V.G.; Kaverina, I.G.; Korobtsov, V.V.; Saranin, A.A.; Zotov, A.V. Thermal annealing behaviour of Si/SiO₂ structures. *Thin Solid Films* **1986**, *135*, 99–105. [[CrossRef](#)]
31. Deal, B.E. *The Physics and Chemistry of SiO₂ and the Si-SiO₂ Interface*, 1st ed.; Springer: New York, NY, USA, 1988; p. 570.
32. Garnica-Romo, M.G.; Yañez-Limón, J.M.; Villicaña, M.; Pérez-Robles, J.F.; Zamorano-Ulloa, R.; González-Hernandez, J. Structural evolution of sol–gel SiO₂ heated glasses containing silver particles. *J. Phys. Chem. Solids* **2004**, *65*, 1045–1052. [[CrossRef](#)]
33. Tahiri, N.; Khouchaf, L.; Elaammani, M.; Louarn, G.; Zegzouti, A.; Daoud, M. Study of the thermal treatment of SiO₂ aggregate. In *IOP Conference Series: Materials Science and Engineering*; IOP Publishing: Bristol, UK, 2014; Volume 62, p. 012002.
34. Zarzycki, J. *Glasses and the Vitreous State*; Cambridge University Press: Cambridge, UK, 1991; p. 533.
35. Rabinovich, E.M. Preparation of glass by sintering. *J. Mater. Sci.* **1985**, *20*, 4259–4297. [[CrossRef](#)]
36. Tański, T.; Matysiak, W.; Krzemiński, Ł.; Jarka, P.; Gołombek, K. Optical properties of thin fibrous PVP/SiO₂ composite mats prepared via the sol-gel and electrospinning methods. *Appl. Surf. Sci.* **2017**, *424*, 184–189. [[CrossRef](#)]
37. Bansal, N.P. Sol-gel synthesis of magnesium oxide-silicon dioxide glass compositions. *J. Am. Ceram. Soc.* **1988**, *71*, 666–672. [[CrossRef](#)]
38. Janssens, W.; Makshina, E.V.; Vanelderen, P.; Clippel, F.D.; Houthoofd, K.; Kerkhofs, S.; Martens, J.A.; Jacobs, P.A.; Sels, B.F. Ternary Ag/MgO-SiO₂ catalysts for the conversion of ethanol into butadiene. *ChemSusChem* **2015**, *8*, 994–1008. [[CrossRef](#)] [[PubMed](#)]
39. Zhang, M.; Gao, M.; Chenab, J.; Yu, Y. Study on key step of 1,3-butadiene formation from ethanol on MgO/SiO₂. *RSC Adv.* **2015**, *5*, 25959–25966. [[CrossRef](#)]
40. Jia, Y.; Wang, B.; Wu, Z.; Zhang, T. Effect of CaO on the reaction process of MgO-SiO₂-H₂O cement pastes. *Mater. Lett.* **2017**, *192*, 48–51. [[CrossRef](#)]
41. Lippincott, E.R.; Valkenburg, A.V.; Weir, C.E.; Bunting, E.N. Infrared studies on polymorphs of silicon dioxide and germanium dioxide. *J. Res. Nat. Bur. Stand.* **1958**, *61*, 61–70. [[CrossRef](#)]
42. Lehmann, A.; Schumann, L.; Hübner, K. Optical phonons in amorphous silicon oxides. II. Calculation of phonon spectra and interpretation of the IR transmission of SiO_x. *Phys. Status Solidi (b)* **1984**, *121*, 505–511. [[CrossRef](#)]

43. Innocenzi, P. Infrared spectroscopy of sol–gel derived silica-based films: A spectra-microstructure overview. *J. Non-Cryst. Solids* **2003**, *316*, 309–319. [[CrossRef](#)]
44. Aguiar, H.; Serra, J.; Gonzalez, P.; León, B. Structural study of sol–gel silicate glasses by IR and Raman spectroscopies. *J. Non-Cryst. Solids* **2009**, *355*, 475–480. [[CrossRef](#)]
45. Klevenz, M.; Wetzel, S.; Möller, M.; Pucci, A. Evaporation and condensation of SiO and SiO₂ studied by infrared spectroscopy. *Appl. Spectrosc.* **2010**, *64*, 298–303. [[CrossRef](#)] [[PubMed](#)]
46. Slimen, F.B.; Zaaboub, Z.; Haouari, M.; Mohamed, N.B.H.; Ouada, H.B.; Chaussedent, S.; Gaumer, N. Effect of CdS nanocrystals on the photoluminescence of Eu³⁺-doped silicophosphate sol gel glass. *RSC Adv.* **2017**, *7*, 14552–14561. [[CrossRef](#)]
47. Morrow, B.A.; McFarlan, A.J. Surface vibrational modes of silanol groups on silica. *J. Phys. Chem. C* **1992**, *96*, 1395–1400. [[CrossRef](#)]
48. Davis, K.M.; Tomozawa, M. An infrared spectroscopic study of water-related species in silica glasses. *J. Non-Cryst. Solids* **1996**, *201*, 177–198. [[CrossRef](#)]
49. Nakagawa, I.; Walter, J.L. Optically active crystal vibrations of the alkalimetal nitrates. *J. Chem. Phys.* **1969**, *51*, 1389–1397. [[CrossRef](#)]
50. Binnemans, K.; Görrler-Walrand, C. Application of the Eu³⁺ ion for site symmetry determination. *J. Rare Earths* **1996**, *14*, 173–180.
51. Görrler-Walrand, C.; Fluyt, L.; Ceulemans, A. Magnetic dipole transitions as standards for Judd–Ofelt parametrization in lanthanide spectra. *J. Chem. Phys.* **1991**, *95*, 3099–3106. [[CrossRef](#)]
52. Jørgensen, C.K.; Judd, B.R. Hypersensitive pseudoquadrupole transitions in lanthanides. *Mol. Phys.* **1964**, *8*, 281–290. [[CrossRef](#)]
53. Campostrini, R.; Carturan, G.; Ferrari, M.; Montagna, M.; Pilla, O. Luminescence of Eu³⁺ ions during thermal densification of SiO₂ gel. *J. Mater. Res.* **1992**, *7*, 745–753. [[CrossRef](#)]
54. Chaussedent, S.; Monteil, A. Molecular dynamics simulation of trivalent europium in aqueous solution: A study on the hydration shell structure. *J. Chem. Phys.* **1996**, *105*, 6532–6537. [[CrossRef](#)]
55. Nogami, M.; Hayakawa, T. Persistent spectral hole burning of sol-gel-derived Eu³⁺-doped SiO₂ glass. *Phys. Rev. B* **1997**, *56*, R14235–R14238. [[CrossRef](#)]
56. Jia, W.Y.; Liu, H.M.; Felofilov, S.P.; Meltzer, R.; Jiao, J. Spectroscopic study of Eu³⁺-doped and Eu³⁺, Y³⁺ codoped SiP₂ sol–gel glasses. *J. Alloys Compd.* **2000**, *311*, 11–15. [[CrossRef](#)]

Sample Availability: Samples of the compounds are currently not available from the authors.



© 2018 by the authors. Licensee MDPI, Basel, Switzerland. This article is an open access article distributed under the terms and conditions of the Creative Commons Attribution (CC BY) license (<http://creativecommons.org/licenses/by/4.0/>).